ACS OMEGA

http://pubs.acs.org/journal/acsodf

Article

Zn^{2+}-Induced Conformational Change Affects the SAM Binding in a Mycobacterial SAM-Dependent Methyltransferase

Soneya Majumdar,[‖] Umang Gupta,[‖] Hariharan V. Chinnasamy, Sathishkumar Laxmipathy, and Saravanan Matheshwaran*

Cite This: *ACS Omega* 2022, 7, 35901−35910

Read Online

ACCESS | Metrics & More | Article Recommendations | Supporting Information

ABSTRACT: Zinc is a cofactor for enzymes involved in DNA replication, peptidoglycan hydrolysis, and pH maintenance, in addition to the transfer of the methyl group to thiols. Here, we discovered a new role of Zn^{2+} as an inhibitor for *S*-adenosyl methionine (SAM) binding in a mycobacterial methyltransferase. Rv1377c is annotated as a putative methyltransferase that is upregulated upon the mitomycin C treatment of *Mycobacterium tuberculosis*. Sequence analysis and experimental validation allowed the identification of distinct motifs responsible for SAM binding. A detailed analysis of the AlphaFold-predicted structure of Rv1377c revealed four cysteine residues capable of coordinating a Zn^{2+} ion located in proximity to the SAM-binding site. Further, experimental studies showed distinct conformational changes upon Zn^{2+} binding to the protein, which compromised its ability to bind SAM. This is the first report wherein Zn^{2+}-driven conformational changes in a methyltransferase undermines its ability to bind SAM.

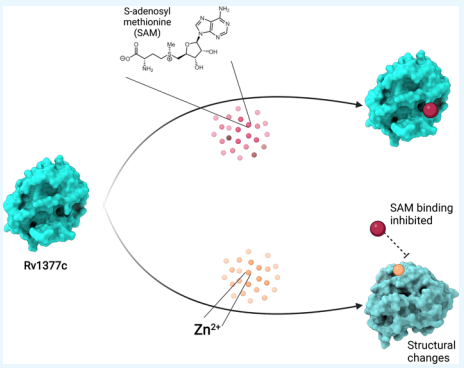

INTRODUCTION

Zinc is the second-most abundant transition metal in living organisms. It plays crucial structural and catalytic roles.[1] Almost 5−6% of proteins in bacteria bind zinc, and these regulate various cellular processes such as glycolysis, DNA replication, biosynthesis of amino acids, peptidoglycan, etc.[2] The role of zinc in catalysis was first revealed in carbonic anhydrases.[3] Subsequently, it was shown that zinc acts as a cofactor for members of six major functional classes of enzymes.[4] Both catalytic and structural roles for zinc have been reported in the *KpnI* restriction endonuclease.[5] Certain phosphatases require three zinc ions, e.g., phospholipase C, while some peptidases require two zinc ions, e.g., amino-peptidases and alkaline phosphatases.[6] The structural role of zinc was first shown in TFIIIA, and a distinct zinc-binding motif termed zinc-finger was consequently identified in several transcription factors.[7,8] Zinc, as a cofactor, is reported in some methyltransferases, such as Ada,[9] and cobalamin-dependent[10] and cobalamin-independent methionine synthase.[11] These proteins employ thiols as nucleophiles. The coordination of these thiols to zinc maintains its reactivity at neutral pH.

Methyltransferases (MTases) catalyze methyl transfer reactions to different substrates such as nucleic acids, proteins, hormones, lipids, small molecules, etc. S-Adenosyl methionine-dependent methyltransferases (SAM-MTase) form the largest group of MTases.[12] These enzymes utilize SAM as a cosubstrate in the reaction. The sequence homology among the various members of this group is limited; however, they do retain a conserved SAM-binding catalytic domain, which is a modified Rossman fold having a central core with a mixed β-sheet sandwiched between α-helices.[13,14] Additional domains that are highly variable both at the sequence and the structural level confer substrate specificity to the MTases. DNA MTases are a critical part of the restriction−modification system in bacteria where they methylate specific DNA sequences of the bacterium, distinguishing them from any incoming foreign DNA.[15] RNA MTases regulate processes such as ribosome assembly, translation initiation, pre-mRNA maturation, etc., by methylating mRNA, tRNA, and rRNA.[16−18] Protein MTases represent a diverse class responsible for protein folding and regulating gene expression.[19] Small-molecule MTases contribute to various metabolic processes that may lead to drug resistance, metal ion toxicity, etc.[20−23] There are 121 methyltransferases identified in *Mycobacterium tuberculosis* (Mtb), of which some are unique to this pathogen.[24] Rv1316c (OGT) and Rv1317c (AlkA) are involved in DNA repair.[25] Rv3263 (MamA), a DNA methylase, was shown to methylate Mtb genomic DNA, which helps mycobacteria to adapt to various physiological stress.[26] DNA MTases in Mtb play significant roles in modulating host epigenetic relations (Rv1988, Rv2966c)[27,28] by methylating the host cell histones

Received: July 19, 2022
Accepted: September 16, 2022
Published: September 27, 2022

and cytosines of non-CpG islands, thereby controlling the host transcriptional machinery. RNA MTases also play a role in virulence (Rv2118)[29] and developing drug resistance (Rv1694-TlyA, Rv2372c)[30,31] in Mtb. Recently Ali et al. showed induced virulence and resistance to antibiotics upon the functional gain of Rv1523, a mycolic acid MTase in *Mycobacterium smegmatis*.[32]

Three percent of the Mtb genome is composed of MTases, most of which are still uncharacterized. Analyzing and characterizing these MTases may help to understand the pathomechanism of Mtb and identify new drug targets. Rv1377c (Uniprot-P71805) is a putative methyltransferase that is induced 13-folds upon mitomycin C treatment.[33,34] It does not possess an SOS box, the DNA sequence where LexA binds and controls expression. However, it is cotranscribed with Rv1378c, which is a putative nuclease.[33] Rv1377c is the only putative methyltransferase under SOS regulation in Mtb.[33] Here, we have shown a unique role for Zn^{2+} in the regulation of cosubstrate binding in Rv1377c.

MATERIALS AND METHODS

Materials. The bacterial strains and vectors used in this study are listed in Table S1 in the Supporting information. Constructs generated and primers used are listed in Table S2 in the Supporting Information, and primers were purchased from ILS and Sigma-Aldrich. The columns used in protein purification were purchased from GE Healthcare Life Sciences. All of the media and reagents were acquired from Hi-Media, Sigma-Aldrich, and SRL. All of the enzymes were procured from New England Biolabs (NEB).

Structure Prediction. The AlphaFold program was obtained from GitHub release and used to predict the structure of Rv1377c (Uniprot-P71805). Later, this structure was also available in the AlphaFold Protein Structure database (using AlphaFold Monomer v2.0 pipeline)[35,36] where three-dimensional (3D) structures of proteins from several model organisms are accessible, including *M. tuberculosis*. The reported model confidence was very high (>90) for this structure.

Cloning, Overexpression, and Purification of Rv1377c Wild Type and Mutants. Rv1377c was cloned using *Nde*I and *Hin*dIII sites in the pET28a(+) vector for 6XHis-tagged proteins and in *Nco*I and *Hin*dIII sites with a stop codon for untagged proteins. Rv1377c mutants (Table S1) were generated using the wild-type construct as a template by employing the overlapping PCR method[37] and confirmed by sequencing (Figure S1). The constructs were expressed in *Escherichia coli* BL21(DE3) cells induced with 0.8 mM IPTG at 37 °C for 4−5 h for both tagged and untagged proteins.

6XHis-Tagged Protein Purification. WT-Rv1377c and mutants (D51A and D74A) were 6XHis-tagged proteins. Cells were lysed in 50 mM Tris−Cl, 10 mM imidazole, 150 mM NaCl (pH 8), and 1 mM PMSF by sonication. Lysates were clarified by centrifugation at 25,000 rpm. Clarified lysates were loaded on a pre-equilibrated Ni-NTA column, washed with buffer comprising 25 mM Tris−Cl, 20 mM imidazole, and 500 mM NaCl (pH 8), and eluted in 100% elution buffer (25 mM Tris−Cl, 500 mM imidazole, 100 mM NaCl, pH 8). The fractions containing the desired protein were combined and loaded onto a Hi-trap Q-sepharose. A continuous gradient of NaCl from 100 mM to 1 M in 25 mM Tris−Cl was used to elute the protein (100% gradient in 30 mL of 1.3 mL elution volume). The protein fractions were pooled and passed through a Superdex 75 size exclusion chromatography column equilibrated with buffer comprising 25 mM Tris−Cl, 100 mM NaCl, and 5% glycerol (pH 8, 0.4 mL/min flow rate in 1 mL elution volume). The protein was stored at −80 °C. All of the assays with SAM were performed on 6XHis-tagged proteins.

Untagged Protein Purification. WT-Rv1377c and cysteine mutants (C54A, C117A, C122A, C149A, and double mutant C117A−C149A) were untagged proteins. Clarified lysates were subjected to ammonium sulfate precipitation (0−20, 20−50, and 50−70%). The precipitates obtained from 20−50 and 50−70% were resuspended in a buffer containing 25 mM Tris−Cl and 75 mM NaCl (pH 8). The suspension was dialyzed for 5 h against the same buffer and then loaded onto a pre-equilibrated Q-sepharose column. A continuous gradient of 100 mM−1 M NaCl in 25 mM Tris−Cl was used to elute the protein. The fractions were analyzed on SDS-PAGE and subsequently pooled and dialyzed in a buffer containing 25 mM Tris−Cl and 75 mM NaCl (pH 8). The dialyzed fractions were loaded onto a pre-equilibrated Mono-Q column. Salt gradient (75 mM to 1 M)-based elution of the protein was performed. The fractions containing the desired protein were pooled, concentrated, and loaded on a Superdex 75 10/300 size exclusion chromatography column equilibrated with a buffer containing 25 mM Tris−Cl, 100 mM NaCl, and 5% glycerol (pH 8). The purified protein was stored at −80 °C. In all of the assays where Zn^{2+} was present, untagged proteins were used. All of the purified protein purification profiles are present in the Supporting Information (Figure S2)

Isothermal Titration Calorimetry (ITC). The affinity of Rv1377c wild type and mutants for SAM and Zn^{2+} was determined using ITC. A MicroCal iTC200 (Malvern Panalytical) was used to perform all of the ITC experiments in a buffer containing 25 mM Tris−Cl and 100 mM NaCl (pH 8). For SAM binding, 50 μM protein was titrated with 1 mM SAM, while for Zn^{2+} binding, 60 μM protein was titrated with 1 mM $ZnCl_2$. For experiments in which SAM binding was monitored in the presence of Zn^{2+}, the ITC buffer was supplemented with 200 μM $ZnCl_2$; however, SAM and protein concentrations were maintained as in the previous experiment; 280 μL of the protein was taken in a sample cell and a syringe was filled with the respective ligand. Then, 2 μL of the ligand was added to the protein for 20 injections at 4 min intervals with a stirring speed of 750 rpm at 25°C. The Microcal Origin 7 platform was used to analyze the data. The ligand was titrated into the buffer, and the heat of dilutions was normalized with an experiment for baseline correction. A "one-set-of-site" model (one binding site of the ligand per protein molecule) was used to determine the stoichiometry (n), binding constant (K), and other thermodynamic parameters.[38] The reciprocal of the binding constant was used to calculate the dissociation constant (K_d). All of the experiments were repeated thrice.

Circular Dichroism Spectroscopy (CD). Secondary structural changes in Rv1377c upon metal ion binding were monitored using CD spectroscopy. Wavelengths from 250 to 200 nm were used to record the CD spectra at 25 °C in a cuvette with a path length of 1 cm using a JASCO J-720 spectropolarimeter. The scan speed was maintained at 50 nm/min, and experiments were conducted in duplicates. Molar ellipticity $[\theta]$ (in deg cm^2 $dmol^{-1}$) was used for plotting the results. The molar ellipticity was determined as follows

$$[\theta] = (100 \times \text{wt} \times \theta)/cl$$

https://doi.org/10.1021/acsomega.2c04555
ACS Omega 2022, 7, 35901−35910

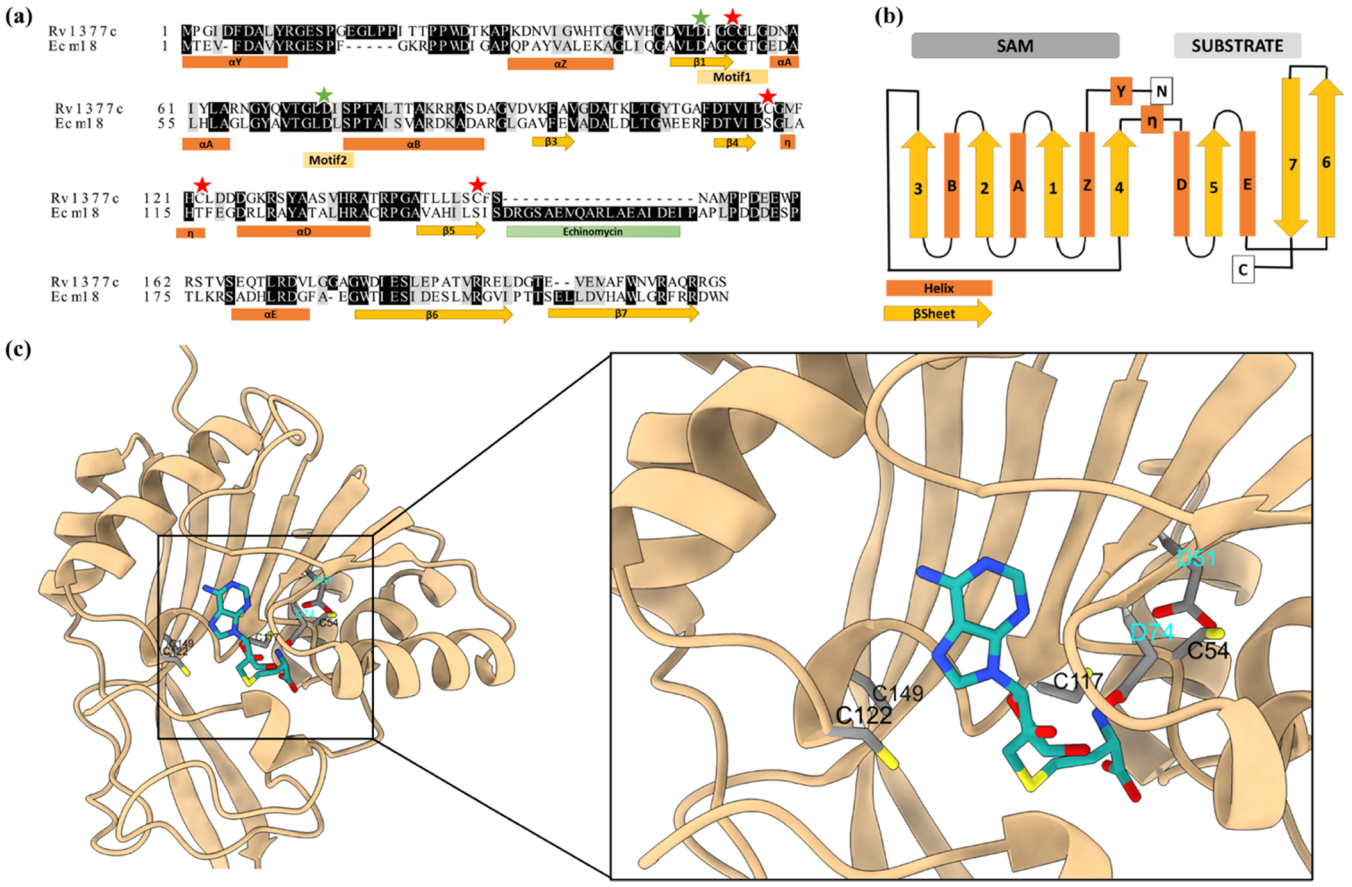

Figure 1. Homology model and structure prediction of Rv1377c. (a) Structure-based alignment of Rv1377c with Ecm18. The conserved regions are shown in black and similar in gray. α-Helices and β-sheets are shown with orange open cylinders and yellow open arrows, respectively. Echinomycin-binding residues are marked with a solid green line. Asp residues are highlighted in green stars, and Cys residues are highlighted in red stars in the alignment. (b) Topological diagram of Rv1377c. (c) AlphaFold predicted the structure of Rv1377c superimposed with PDB: 4NEC to display the *S*-adenosyl homocysteine (SAH, blue) binding site. The aspartates from motif1 and motif2 are shown (cyan). The potential Zn^{2+} coordinating cysteine residues are also displayed (black).

where θ is the ellipticity (in degrees) at a particular wavelength, wt is the weight of the protein, c is the protein concentration (in mg mL^{-1}), and l is the length of the light path (cm). The baseline for all of the samples was corrected. The buffer used contained 10 mM Tris−Cl and 100 mM NaCl (pH 8). The CD experiments were performed with a protein concentration of 6 μM. The molar ellipticities were plotted as a function of wavelength using OriginPro 9.1. Further, the thermal stability of Rv1377c was examined in the presence of Zn^{2+} (100 μM), SAM (60 μM), or both. The secondary structural changes in the protein were evaluated with increasing temperature (25−70 °C) at 220 nm. The percentage of the unfolded protein[39] was plotted against the increase in temperature using OriginPro 9.1.

Proteinase K Cleavage of Rv1377c. Proteinase K cleavage of Rv1377c was carried out in the presence of Zn^{2+} (200 μM), SAM (400 μM), or both; 2 mg/mL protein was preincubated for 15 min with ligands in a buffer comprising 25 mM Tris−Cl and 100 mM NaCl (pH 8), and 1% proteinase K was used for the assay at 37 °C. At specified time points, 5 μL of the sample was retrieved, and proteinase K was inactivated using 1 mM PMSF and 5X SDS dye. The samples were analyzed on 15% SDS-PAGE.

RESULTS

Rv1377c: A SAM-Dependent MTase. PSI-BLAST search with the Rv1377c sequence against the PDB database reveals significant sequence homology with Ecm18, a SAM-dependent MTase from *Streptomyces lasaliensis*, which converts a disulfide bridge in the echinomycin precursor triostin A to the thioacetal linkage.[40] A pairwise sequence alignment of Rv1377c and Ecm18 shows a sequence identity of 39% and a similarity of 54%. Although the overall sequence similarity is high, a short stretch of 19aa, which binds echinomycin in Ecm18, is missing in Rv1377c (Figure 1a). The crystal structure of Ecm18 complexed with the reaction byproduct *S*-adenosyl-L-homocysteine (SAH) is available.[40] We generated a model for Rv1377c using AlphaFold[35,36] (Figure 1c).

Rv1377c exhibits a typical N-terminal SAM-MTase fold having alternate secondary structures, which occur as seven-stranded β sheets with three α helices on either side (Figure 1b). The overall fold resembles the Class I SAM-MTases specific for DNA and small-molecule methyltransferases. In these MTases, the SAM-binding domain comprises the N-terminal half of the protein, while the C-terminus of the protein binds substrates. Rv1377c does not have any significant insertions in the C-terminus. Such domain insertions at the C-terminus are common to nucleic acid and protein MTases for substrate binding.[41] Hence, the overall topology considering

https://doi.org/10.1021/acsomega.2c04555
ACS Omega 2022, 7, 35901−35910

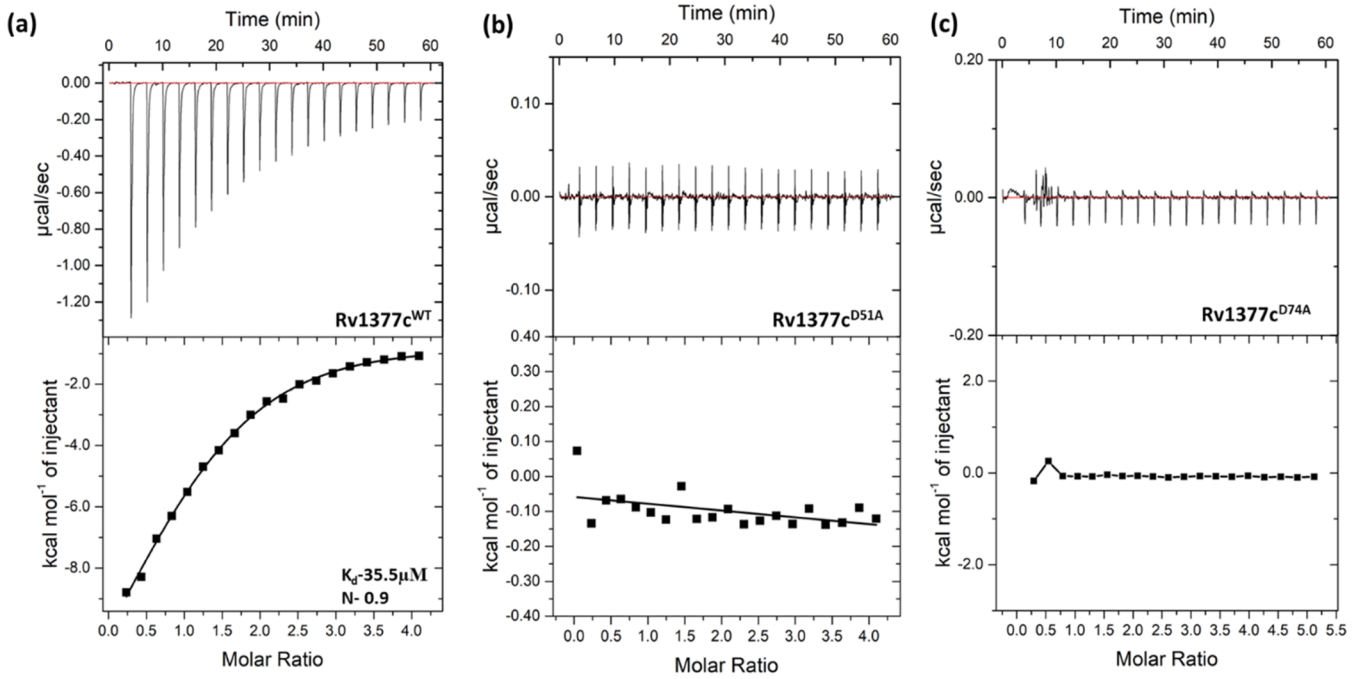

Figure 2. ITC analysis of SAM binding to Rv1377c. Representative ITC profiles are shown here. The top panel in each shows the heat change in the raw data and the bottom panels show the binding isotherms of Rv1377c, and mutants generated by plotting the combined heat peaks on injecting SAM to (a) Rv1377c^{WT}, (b) Rv1377c^{D51A}, and (c) Rv1377c^{D74A}.

Table 1. Thermodynamic Parameters for the Association of Rv1377c and Its Mutants for SAM Binding[a]

protein	N	K_a (M^{-1})	K_d (μM)	ΔH (kcal mol^{-1})	ΔS (cal mol^{-1} deg^{-1})	ΔG (kJ)
SAM Binding in the Absence of Zn^{2+}						
WT	1.10 ± 0.05	(2.81 ± 0.17) × 10^4	35.5	−17.56 ± 1.16	−39	−24.82
C54A	0.85 ± 0.08	(2.21 ± 0.77) × 10^4	47	−8.47 ± 1.14	−7.8	−25.7
C149A	1.11 ± 0.03	(2.93 ± 0.57) × 10^4	34.1	−13.29 ± 0.26	−24.2	−25.42
C117A/C149A	0.97 ± 0.40	(1.36 ± 0.29) × 10^4	72	−12.77 ± 5.82	−23.9	−23.62
SAM Binding in the Presence of Zn^{2+}						
WT						
C54A	1.15 ± 0.35	(3.20 ± 0.37) × 10^4	31	−4.40 ± 1.90	−5.86	−11.09
C149A	0.91 ± 0.19	(2.68 ± 0.57) × 10^4	37	−32.85 ± 2.0	−89.9	−25.3
C117A/C149A	0.91 ± 0.03	(6.09 ± 0.12) × 10^4	16.4	−13.12 ± 0.86	−22.1	−27.3

[a] N, no. of binding sites; K_a, association constant; K_d, dissociation constant; ΔH, enthalpy change; ΔS, entropy change; ΔG, Gibbs free energy.

the small substrate-binding site of Rv1377c closely resembles that of a small-molecule MTase.[12,42]

Based on the sequence alignment and structural comparison between Ecm18 and Rv1377c, the residues that could allow SAM binding at the active site of Rv1377c were predicted (Figure 1a,c). A noteworthy feature of the SAM-MTases is the poor conservation of residues involved in SAM binding, although SAM binds to the same position in the Rossman fold of the MTase variations existing in the interactions that stabilize SAM at the active site. Hallmarks of the SAM-binding motif in MTases include a glycine-rich sequence in the first β-strand, which interacts with methionine, and a conserved acidic residue in the second β-strand, which interacts with ribose sugar.[43,44] We identified two prototypical, highly conserved SAM-binding motifs. Motif1 is a glycine-rich sequence DXGXGXG between β1 and αA, which interacts with methionine, while motif2 is an acidic loop (DIS) between β2 and αB, which interacts with ribose sugar (Figure 1a,c).

We checked the binding of purified recombinant Rv1377c with SAM using ITC. Rv1377c binds to SAM with 1:1 stoichiometry and an affinity of 35.5 μM (Figure 2). Further, to identify the SAM-binding residues, point mutants of Rv1377c were generated and tested for SAM binding using ITC. D51 from motif1 and D74 from motif2 were mutated to alanine and subjected to SAM binding. The SAM-binding properties of both D51A and D74A mutants were abrogated (Figure 2 and Table 1), suggesting the roles of motif1 and motif2 in SAM binding.

Rv1377c: A Zinc Metalloenzyme. An interesting feature in the Rv1377c structure is the presence of four cysteine residues (C54, C117, C122, and C149) in the vicinity of the predicted SAM-binding site (Figure 1a,c). These four cysteines are highly conserved among a number of pathogenic mycobacterial species, but two of these cysteines are absent in *M. smegmatis* (Figure S2). We tested whether Zn^{2+} induces any significant structural changes in the protein.

Toward this, circular dichroism (CD) studies were performed with Zn^{2+} and other metal ions (Mg^{2+}, Mn^{2+}, and Ca^{2+} as control). The far-ultraviolet (UV) CD spectra of Rv1377c exhibit two negative peaks at 208 and 220 nm,

https://doi.org/10.1021/acsomega.2c04555
ACS Omega 2022, 7, 35901−35910

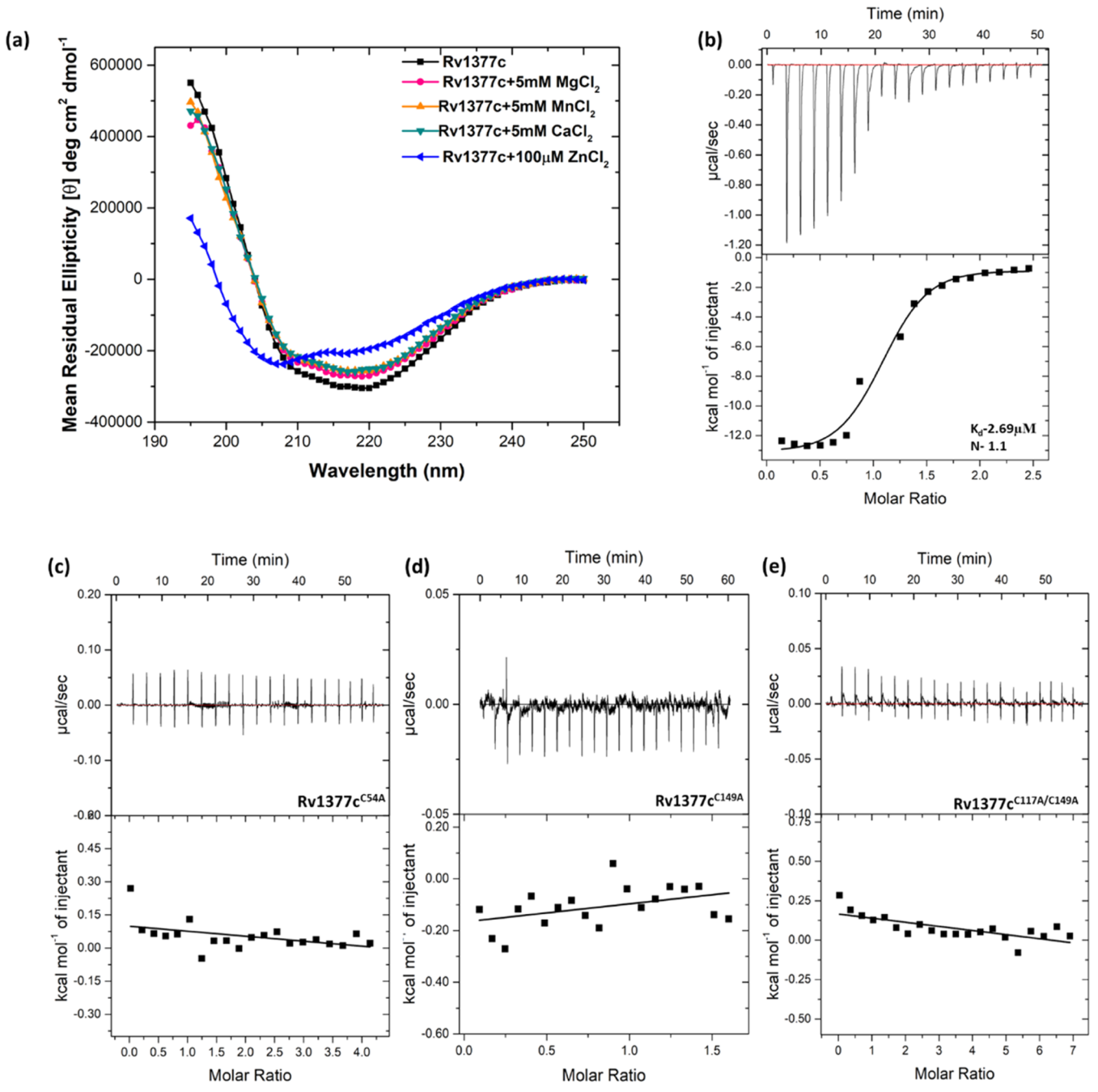

Figure 3. Effect of the Zn^{2+} ion on the structure and stability of Rv1377c. (a) Average of three far-UV CD spectra of purified Rv1377c (6 μM, black square), and changes in the structure studied in the presence of divalent metal ions: 5 mM $MgCl_2$ (red circle), 5 mM $MnCl_2$ (orange upright triangle), 5 mM $CaCl_2$ (green inverted triangle), and 100 μM $ZnCl_2$ (blue left triangle) at 25 °C. The mean residual ellipticity has been plotted. (b−e) Representative ITC profiles are shown. The top panel shows the raw data, and the bottom panel shows the binding isotherms generated by plotting the integrated heat peaks on injecting Zn^{2+} in Rv1377c WT and mutants (b) Rv1377c^{WT}, (c) Rv1377c^{C54A}, (d) Rv1377c^{C149A}, and (e) Rv1377c$^{C117A/C149A}$.

atypical for helices. In the presence of Zn^{2+}, there is a decrease in the overall helicity of the protein, indicating secondary structural changes, while other metal ions such as Mg^{2+}, Mn^{2+}, and Ca^{2+} induced no significant differences in the CD spectra (Figure 3a). Next, we determined the affinity of Rv1377c for Zn^{2+} using ITC. Our results indicate that Rv1377c binds Zn^{2+} with a stoichiometry of 1:1 and an affinity of 2.69 μM (Figure 3b). To confirm that the identified cysteine residues coordinate Zn^{2+}, we generated Rv1377c single-cysteine mutants (C54A, C117A, C122A, and C149A) and a double mutant (C117A−C149A). We found that the elution profile for the cysteine mutant proteins was distinct from that of wild-type proteins (Figure S3a). To confirm whether these differences were due to any secondary structural changes, CD spectroscopy was performed. The CD spectra confirmed that there were no mutation-induced secondary structural changes (Figure S3b). These mutant proteins were checked for Zn^{2+} andSAM binding using ITC (Figures 3 and S4). In tune with our predictions, the Rv1377c cysteine mutants failed to bind Zn^{2+}, but the SAM-binding property of the proteins was

https://doi.org/10.1021/acsomega.2c04555
ACS Omega 2022, 7, 35901−35910

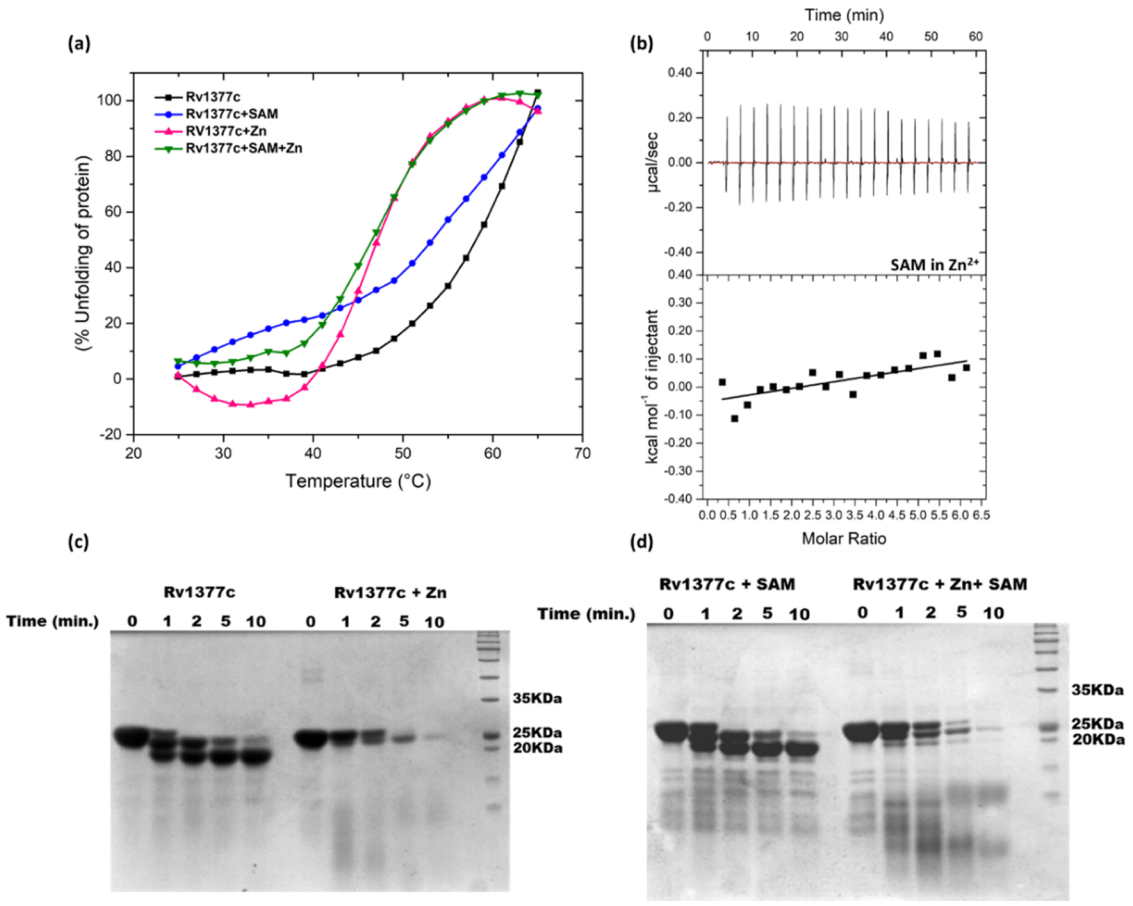

Figure 4. Effect of the Zn^{2+} metal ion on SAM binding of Rv1377c. (a) Thermal stability of Rv1377c without (black square) and with 100 μM $ZnCl_2$ (pink upright triangle), 60 μM SAM (blue circle), and 60 μM SAM + 100 μM $ZnCl_2$ (green inverted triangle). The percent unfolded protein as a Boltzmann sigmoid function at 220 nm is plotted against temperature. (b) Abrogated binding of SAM to Rv1377c in the presence of Zn^{2+} as observed by ITC. The binding isotherm was generated by injecting SAM to Rv1377c and incubated with Zn^{2+}. (c, d) Proteinase K cleavage assay. The protease cleavage assay was performed in the presence of Zn^{2+}, SAM, and both ligands at different time intervals. Rv1377c degrades into a fragment with a size of ~20 kDa, which is consistent in the presence of SAM, whereas in the presence of Zn^{2+}, Rv1377c completely degrades (even in the presence of SAM).

unaffected with affinities comparable to those of wild-type proteins (Table 1). We conclude that Rv1377c is a metalloenzyme with a zinc-binding motif comprising four cysteine residues.

Zn^{2+} Inhibits SAM Binding in Rv1377c. Two of the cysteine residues (C54 and C117), which coordinate Zn^{2+}, occur in motif1 (Figure 1) and in the short helical insertion observed between β4 and αD. We anticipated that Zn^{2+} binding to these cysteines might affect SAM binding to Rv1377c. We tested this using ITC, CD spectroscopy, and protease cleavage assays. ITC experiments were conceived to investigate whether the addition of Zn^{2+} affects SAM binding. We observed that the presence of Zn^{2+} altogether abolished SAM binding to Rv1377c (Figure 4b). However, Rv1377c cysteine mutants bind SAM with affinities comparable (Table 1) to that of the wild type in the presence of Zn^{2+}. Hence, specific coordination of Zn^{2+} by the identified cysteine residues prevents SAM binding to Rv1377c. To investigate whether this effect is associated with significant structural changes, protein stability was monitored at 220 nm with increasing temperature, in the presence and absence of Zn^{2+} and SAM, using CD spectroscopy. The percent unfolded protein was plotted against temperature to determine the melting temperature of the protein (T_m). The T_m of Rv1377c (63.6 °C) marginally increases in the presence of SAM (66 °C); however, in the presence of Zn^{2+}, T_m decreases significantly to 46.6 °C (Figure 4 a). Further, we observed that upon the addition of SAM, the destabilization induced by Zn^{2+} is not rescued, and T_m is 47 °C. These observations indicate that Zn^{2+} binding destabilizes the SAM-binding pocket of Rv1377c. For further investigation, the proteinase K cleavage assay of Rv1377c was performed in the presence of Zn^{2+} and SAM. Proteinase K cleavage of Rv1377c in the presence and absence of SAM revealed a fragment 20 kDa in size, which was highly stable to proteolytic cleavage. This could be the SAM-binding domain, which is a modified Rossman fold having a size of ~20 kDa. This implies that the SAM-binding pocket forms a stable domain, unaffected by proteinase K treatment, even in the absence of bound SAM (Figure 4d). However, proteinase K cleavage of Rv1377c in the presence of Zn^{2+} leads to extensive cleavage of the protein with no stable fragment. A similar observation was made when Rv1377c was cleaved with proteinase K in the presence of SAM and Zn^{2+} (Figure 4c,d). Overall, our observations establish that Zn^{2+} binding to the cysteine residues destabilizes the SAM-binding pocket in Rv1377c, preventing the cosubstrate from binding (Figure 5).

https://doi.org/10.1021/acsomega.2c04555
ACS Omega 2022, 7, 35901−35910

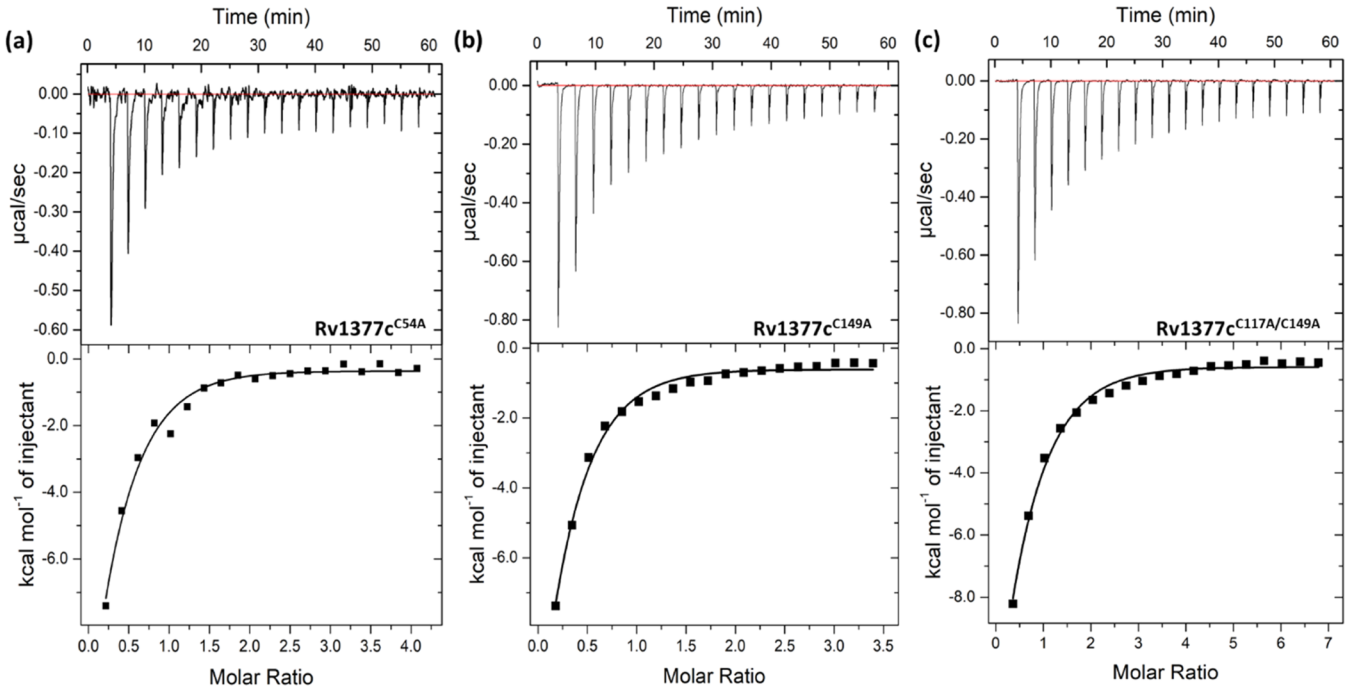

Figure 5. Analysis of SAM binding to Rv1377c cysteine mutants in the presence of Zn^{2+}. ITC was performed to check SAM binding for the cysteine mutants of Rv1377c in the presence of Zn^{2+}. The top panel in each shows the raw data and the bottom panels show the binding isotherms of Rv1377c mutants created by plotting the integrated heat peaks by injecting SAM in the presence of Zn^{2+} for (a) Rv1377c^{C54A}, (b) Rv1377c^{C149A}, and (c) Rv1377c$^{C117A/C149A}$.

DISCUSSION

Rv1377c is a putative transferase of Mtb induced upon mitomycin C treatment of cells.[33,34] It has been established through microarray studies that it is among the highly induced genes during the SOS response of Mtb.[33,34] In the current study, we showed that Rv1377c belongs to the AdoMet superfamily of methyltransferases that employ *S*-adenosyl methionine (SAM) as a cosubstrate. It shares a significant sequence identity with antibiotic methyltransferase Ecm18, responsible for converting triostin A to echinomycin.[40] We predicted the structure of Rv1377c using AlphaFold. Sequence and structural analysis allowed identification and subsequent validation of the SAM-binding active site. Nucleic acid and protein methyltransferases usually harbor additional insertions at the C-terminal substrate-binding region to accommodate the substrate.[45] On the contrary, Rv1377c has a small substrate-binding pocket, suggesting that it could be a small molecule or lipid methyltransferase.

Interestingly, we identified a probable Zn^{2+}-binding site in Rv1377c comprising four cysteine residues. ITC experiments reveal that Zn^{2+} binding to the protein abolishes its ability to bind SAM. The above observation is explained by the CD and proteinase K cleavage experiments. CD analysis indicates that Zn^{2+} destabilizes the secondary structure of Rv1377c, which might lead to the inability to bind SAM. In the proteinase K cleavage assay with Rv1377c in the presence and absence of SAM, it is observed that a 20 kDa protein fragment persists, which is highly stable to proteolytic degradation. This could be the SAM-binding domain, which is a modified Rossman fold having a size of ∼20 kDa. It further ascertains that the SAM-binding pocket forms a stable domain, unaffected by proteinase K treatment, even in the absence of bound SAM. Upon proteinase K cleavage of Rv1377c in the presence of Zn^{2+}, this stable domain is no longer observed, and the total protein is degraded with time. This clearly indicates that Zn^{2+} destabilizes the SAM-binding domain, leading to the loss of binding.

Zn^{2+}−cysteine complexes are involved in structural, catalytic, regulatory, storage, and transport roles.[46,47] In addition to the catalytic and structural roles, Zn^{2+}-mediated inhibition of enzymes is an evolving theme believed to be critical for regulating metabolism and signal transduction.[48,49] Several eukaryotic enzymes, which do not require Zn^{2+} as a cofactor, are known to be inhibited by the metal ion.[50] They include enzymes of the glycolytic pathway, certain proteases, and tyrosine phosphatase. The Zn^{2+}-mediated mechanism of inhibition has been elucidated for a few of them. Zn^{2+} acts as an allosteric inhibitor of fructose 1,6-bisphosphatase, which has a distinct zinc-binding site.[51] Similar allosteric inhibition has been reported in the case of a protease, caspase-6.[52] However, in caspase-9, Zn^{2+}-mediated inhibition is due to the metal ion coordinated to the catalytic dyad.[53] In prokaryotes, very few enzymes exhibiting Zn^{2+}-mediated inhibition are reported, e.g., *E. coli* phenylalanyl-tRNA synthetase.[54] Further, MTases employing Zn^{2+} for catalysis were reported earlier.[55,56] Methionine synthase (MTR) and betaine homocysteine methyltransferase (BHMT) are Zn^{2+}-dependent DNA MTases in humans.[57] Rv1377c, by far, is the first MTase in which Zn^{2+}-mediated inhibition is observed.

Rv1377c ortholog occurs in all of the pathogenic species of Mycobacterium. It is absent in the mycobacterial species, which are opportunistic pathogens and nonpathogens except for *M. smegmatis*. Further, Rv1377c is the only MTase under SOS regulation in Mtb.[33] SOS response is a very efficient strategy employed by bacteria to overcome stress conditions. This indicates that Rv1377c might also have a role in the survival of Mtb during stress. Mtb encounters extremely hostile conditions within the macrophage but successfully survives,

https://doi.org/10.1021/acsomega.2c04555
ACS Omega 2022, 7, 35901−35910

indicating its efficient counteracting ability. One of the approaches to restrict a pathogen within the host is to sequester metal ions, which serve as cofactors for several essential enzymes.[58] Important to note that within the macrophage, reactive nitrogen and oxygen species are generated to stop the growth of bacteria.[59] These reactive nitrogen and oxygen species are known to attack the cysteine thiols that may lead to Zn^{2+} mobilization.[60,61] We foresee that during such conditions, the MTase activity of Rv1377c might be activated.

■ ASSOCIATED CONTENT

Supporting Information

The Supporting Information is available free of charge at https://pubs.acs.org/doi/10.1021/acsomega.2c04555.

Details of bacterial strains and plasmids used in the study; primers used for the generation of constructs; plasmids and constructs generated in this study; particulars of Rv1377c protein mutations used in this study; mutants generated for the study; multiple sequence alignment results of Rv1377c with other mycobacterial species' proteins; characterization of cysteine mutants on the basis of size exclusion chromatography and circular dichroism spectroscopy; and SAM-binding analysis of cysteine mutants by isothermal titration calorimetry (PDF)

Accession Codes

Rv1377c: P71805.

■ AUTHOR INFORMATION

Corresponding Author

Saravanan Matheshwaran − *Department of Biological Sciences and Bioengineering, Indian Institute of Technology, Kanpur 208016 Uttar Pradesh, India; Center for Environmental Science and Engineering and Mehta Family Centre for Engineering in Medicine, Indian Institute of Technology, Kanpur 208016 Uttar Pradesh, India;* orcid.org/0000-0001-6762-9928; Phone: 91-512-259-4066; Email: saran@iitk.ac.in; Fax: 91-512-259-4010

Authors

Soneya Majumdar − *Department of Biological Sciences and Bioengineering, Indian Institute of Technology, Kanpur 208016 Uttar Pradesh, India*

Umang Gupta − *Department of Biological Sciences and Bioengineering, Indian Institute of Technology, Kanpur 208016 Uttar Pradesh, India*

Hariharan V. Chinnasamy − *Department of Biological Sciences and Bioengineering, Indian Institute of Technology, Kanpur 208016 Uttar Pradesh, India*

Sathishkumar Laxmipathy − *Department of Biological Sciences and Bioengineering, Indian Institute of Technology, Kanpur 208016 Uttar Pradesh, India*

Complete contact information is available at: https://pubs.acs.org/10.1021/acsomega.2c04555

Author Contributions

‖S.M. and U.G. contributed equally to this work. All authors have approved the final version of the manuscript.

Notes

The authors declare no competing financial interest.

■ ACKNOWLEDGMENTS

The authors are thankful to the CD facility at IIT Kanpur and CDRI Lucknow for permitting the usage of the instrument. U.G. and H.V.C. acknowledge the Ministry of Human Resource Development, Government of India, for the fellowship. Dr. Appu Kumar Singh is acknowledged for the critical reading of the manuscript. ICMR (52/03/2020-BIO/BMS) and SERB (EMR2017/004846) are acknowledged for funding.

■ ABBREVIATIONS

SAM, *S*-adenosyl methionine; SAH, *S*-adenosyl homocysteine; MTase, methyltransferases; ITC, isothermal calorimetry; CD, circular dichroism

■ REFERENCES

(1) Porcheron, G.; Garénaux, A.; Proulx, J.; Sabri, M.; Dozois, C. M. Iron, Copper, Zinc, and Manganese Transport and Regulation in Pathogenic Enterobacteria: Correlations between Strains, Site of Infection and the Relative Importance of the Different Metal Transport Systems for Virulence. *Front. Cell. Infect. Microbiol.* **2013**, *3*, No. 90.

(2) Andreini, C.; Banci, L.; Bertini, I.; Rosato, A. Zinc through the Three Domains of Life. *J. Proteome Res.* **2006**, *5*, 3173−3178.

(3) Keilin, D.; Mann, T. Carbonic Anhydrase. Purification and Nature of the Enzyme. *Biochem. J.* **1940**, *34*, 1163−1176.

(4) McCall, K. A.; Huang, C. C.; Fierke, C. A. Function and Mechanism of Zinc Metalloenzymes. *J. Nutr.* **2000**, *130*, 1437S−1446S.

(5) Saravanan, M.; Vasu, K.; Ghosh, S.; Nagaraja, V. Dual Role for Zn 2+ in Maintaining Structural Integrity and Induce DNA Sequence Specificity in a Promiscuous Endonuclease. *J. Biol. Chem.* **2007**, DOI: 10.1074/jbc.M705927200.

(6) Bertini, I.; Sigel, A. *Handbook on Metalloproteins*, 1st ed.; CRC Press: Boca Raton, 2001; p 1108.

(7) Miller, J.; McLachlan, A. D.; Klug, A. Repetitive Zinc-Binding Domains in the Protein Transcription Factor IIIA from Xenopus Oocytes. *EMBO J.* **1985**, *4*, 1609−1614.

(8) Hanas, J. S.; Hazuda, D. J.; Bogenhagen, D. F.; Wu, F. Y.; Wu, C. W. Xenopus Transcription Factor A Requires Zinc for Binding to the 5 S RNA Gene. *J. Biol. Chem.* **1983**, *258*, 14120−14125.

(9) Myers, L. C.; Terranova, M. P.; Nash, H. M.; Markus, M. A.; Verdine, G. L. Zinc Binding by the Methylation Signaling Domain of the *Escherichia coli* Ada Protein. *Biochemistry* **1992**, *31*, 4541−4547.

(10) Goulding, C. W.; Matthews, R. G. Cobalamin-Dependent Methionine Synthase from *Escherichia coli*: Involvement of Zinc in Homocysteine Activation. *Biochemistry* **1997**, *36*, 15749−15757.

(11) González, J. C.; Peariso, K.; Penner-Hahn, J. E.; Matthews, R. G. Cobalamin-Independent Methionine Synthase from *Escherichia coli*: A Zinc Metalloenzyme. *Biochemistry* **1996**, *35*, 12228−12234.

(12) Abdelraheem, E.; Thair, B.; Varela, R. F.; Jockmann, E.; Popadić, D.; Hailes, H. C.; Ward, J. M.; Iribarren, A. M.; Lewkowicz, E. S.; Andexer, J. N.; Hagedoorn, P.-L.; Hanefeld, U. Methyltransferases, Functions and Applications. *ChemBioChem* **2022**, *23*, No. e202200212.

(13) Kozbial, P. Z.; Mushegian, A. R. Natural History of S-Adenosylmethionine-Binding Proteins. *BMC Struct. Biol.* **2005**, *5*, No. 19.

(14) Chouhan, B. P. S.; Maimaiti, S.; Gade, M.; Laurino, P. Rossmann-Fold Methyltransferases: Taking a "*β*-Turn" around Their Cofactor, S-Adenosylmethionine. *Biochemistry* **2019**, *58*, 166−170.

(15) Wilson, G. G.; Murray, N. E. Restriction and Modification Systems. *Annu. Rev. Genet.* **1991**, *25*, 585−627.

(16) Shatkin, A. J. Capping of Eucaryotic MRNAs. *Cell* **1976**, *9*, 645−653.

(17) Shatkin, A. J.; Manley, J. L. The Ends of the Affair: Capping and Polyadenylation. *Nat. Struct. Biol.* **2000**, *7*, 838−842.

(18) Bussiere, D. E.; Muchmore, S. W.; Dealwis, C. G.; Schluckebier, G.; Nienaber, V. L.; Edalji, R. P.; Walter, K. A.; Ladror, U. S.; Holzman, T. F.; Abad-Zapatero, C. Crystal Structure of ErmC′, an RRNA Methyltransferase Which Mediates Antibiotic Resistance in Bacteria. *Biochemistry* **1998**, *37*, 7103−7112.
(19) Visick, J. E.; Clarke, S. Repair, Refold, Recycle: How Bacteria Can Deal with Spontaneous and Environmental Damage to Proteins. *Mol. Microbiol.* **1995**, *16*, 835−845.
(20) Cook, R. J.; Horne, D. W.; Wagner, C. Effect of Dietary Methyl Group Deficiency on One-Carbon Metabolism in Rats. *J. Nutr.* **1989**, *119*, 612−617.
(21) Scheuermann, T. H.; Lolis, E.; Hodsdon, M. E. Tertiary Structure of Thiopurine Methyltransferase from Pseudomonas Syringae, a Bacterial Orthologue of a Polymorphic, Drug-Metabolizing Enzyme. *J. Mol. Biol.* **2003**, *333*, 573−585.
(22) Ball, P.; Knuppen, R.; Haupt, M.; Breuer, H. Interactions between Estrogens and Catechol Amines III. Studies on the Methylation of Catechol Estrogens, Catechol Amines and Other Catechols by the Catechol-o-Methyltransferase of Human Liver. *J. Clin. Endocrinol. Metab.* **1972**, *34*, 736−746.
(23) Prigent-Combaret, C.; Sanguin, H.; Champier, L.; Bertrand, C.; Monnez, C.; Colinon, C.; Blaha, D.; Ghigo, J. M.; Cournoyer, B. The Bacterial Thiopurine Methyltransferase Tellurite Resistance Process Is Highly Dependent upon Aggregation Properties and Oxidative Stress Response. *Environ. Microbiol.* **2012**, *14*, 2645−2660.
(24) Grover, S.; Gupta, P.; Kahlon, P. S.; Goyal, S.; Grover, A.; Dalal, K.; Sabeeha; Ehtesham, N. Z.; Hasnain, S. E. Analyses of Methyltransferases across the Pathogenicity Spectrum of Different Mycobacterial Species Point to an Extremophile Connection. *Mol. Biosyst.* **2016**, *12*, 1615−1625.
(25) Durbach, S. I.; Springer, B.; Machowski, E. E.; North, R. J.; Papavinasasundaram, K. G.; Colston, M. J.; Böttger, E. C.; Mizrahi, V. DNA Alkylation Damage as a Sensor of Nitrosative Stress in *Mycobacterium tuberculosis*. *Infect. Immun.* **2003**, *71*, 997−1000.
(26) Shell, S. S.; Prestwich, E. G.; Baek, S.-H.; Shah, R. R.; Sassetti, C. M.; Dedon, P. C.; Fortune, S. M. DNA Methylation Impacts Gene Expression and Ensures Hypoxic Survival of *Mycobacterium tuberculosis*. *PLoS Pathog.* **2013**, *9*, No. e1003419.
(27) Yaseen, I.; Kaur, P.; Nandicoori, V. K.; Khosla, S. Mycobacteria Modulate Host Epigenetic Machinery by Rv1988 Methylation of a Non-Tail Arginine of Histone H3. *Nat. Commun.* **2015**, *6*, No. 8922.
(28) Sharma, G.; Upadhyay, S.; Srilalitha, M.; Nandicoori, V. K.; Khosla, S. The Interaction of Mycobacterial Protein Rv2966c with Host Chromatin Is Mediated through Non-CpG Methylation and Histone H3/H4 Binding. *Nucleic Acids Res.* **2015**, *43*, 3922−3937.
(29) Varshney, U.; Ramesh, V.; Madabushi, A.; Gaur, R.; Subramanya, H. S.; RajBhandary, U. L. *Mycobacterium tuberculosis* Rv2118c Codes for a Single-Component Homotetrameric M1A58 TRNA Methyltransferase. *Nucleic Acids Res.* **2004**, *32*, 1018−1027.
(30) Witek, M. A.; Kuiper, E. G.; Minten, E.; Crispell, E. K.; Conn, G. L. A Novel Motif for S-Adenosyl-l-Methionine Binding by the Ribosomal RNA Methyltransferase TlyA from *Mycobacterium tuberculosis*. *J. Biol. Chem.* **2017**, *292*, 1977−1987.
(31) Kumar, A.; Kumar, S.; Taneja, B. The Structure of Rv2372c Identifies an RsmE-like Methyltransferase from *Mycobacterium tuberculosis*. *Acta Crystallogr., Sect. D: Biol. Crystallogr.* **2014**, *70*, 821−832.
(32) Ali, S.; Ehtram, A.; Arora, N.; Manjunath, P.; Roy, D.; Ehtesham, N. Z.; Hasnain, S. E. The *M. Tuberculosis* Rv1523 Methyltransferase Promotes Drug Resistance Through Methylation-Mediated Cell Wall Remodeling and Modulates Macrophages Immune Responses. *Front. Cell. Infect. Microbiol.* **2021**, *11*, No. 622487.
(33) Rand, L.; Hinds, J.; Springer, B.; Sander, P.; Buxton, R. S.; Davis, E. O. The Majority of Inducible DNA Repair Genes in *Mycobacterium tuberculosis* Are Induced Independently of RecA. *Mol. Microbiol.* **2003**, *50*, 1031−1042.
(34) Brzostek, A.; Płociński, P.; Minias, A.; Ciszewska, A.; Gąsior, F.; Pawełczyk, J.; Dziadek, B.; Słomka, M.; Dziadek, J. Dissecting the RecA-(In)Dependent Response to Mitomycin C in *Mycobacterium tuberculosis* Using Transcriptional Profiling and Proteomics Analyses. *Cells* **2021**, *10*, No. 1168.
(35) Jumper, J.; Evans, R.; Pritzel, A.; Green, T.; Figurnov, M.; Ronneberger, O.; Tunyasuvunakool, K.; Bates, R.; Žídek, A.; Potapenko, A.; Bridgland, A.; Meyer, C.; Kohl, S. A. A.; Ballard, A. J.; Cowie, A.; Romera-Paredes, B.; Nikolov, S.; Jain, R.; Adler, J.; Back, T.; Petersen, S.; Reiman, D.; Clancy, E.; Zielinski, M.; Steinegger, M.; Pacholska, M.; Berghammer, T.; Bodenstein, S.; Silver, D.; Vinyals, O.; Senior, A. W.; Kavukcuoglu, K.; Kohli, P.; Hassabis, D. Highly Accurate Protein Structure Prediction with AlphaFold. *Nature* **2021**, *596*, 583−589.
(36) Varadi, M.; Anyango, S.; Deshpande, M.; Nair, S.; Natassia, C.; Yordanova, G.; Yuan, D.; Stroe, O.; Wood, G.; Laydon, A.; Zídek, A.; Green, T.; Tunyasuvunakool, K.; Petersen, S.; Jumper, J.; Clancy, E.; Green, R.; Vora, A.; Lutfi, M.; Figurnov, M.; Cowie, A.; Hobbs, N.; Kohli, P.; Kleywegt, G.; Birney, E.; Hassabis, D.; Velankar, S. NAR Breakthrough Article AlphaFold Protein Structure Database: Massively Expanding the Structural Coverage of Protein-Sequence Space with High-Accuracy Models. *Nucleic Acids Res.* **2021**, *50*, D439−D44.
(37) Hilgarth, R. S.; Lanigan, T. M. Optimization of Overlap Extension PCR for Efficient Transgene Construction. *MethodsX* **2020**, *7*, No. 100759.
(38) Freyer, M. W.; Lewis, E. A. Isothermal Titration Calorimetry: Experimental Design, Data Analysis, and Probing Macromolecule/Ligand Binding and Kinetic Interactions. *Methods Cell Biol.* **2008**, *84*, 79−113.
(39) Greenfield, N. J. Using Circular Dichroism Collected as a Function of Temperature to Determine the Thermodynamics of Protein Unfolding and Binding Interactions. *Nat. Protoc.* **2006**, *1*, 2527−2535.
(40) Hotta, K.; Keegan, R. M.; Ranganathan, S.; Fang, M.; Bibby, J.; Winn, M. D.; Sato, M.; Lian, M.; Watanabe, K.; Rigden, D. J.; Kim, C. Y. Conversion of a Disulfide Bond into a Thioacetal Group during Echinomycin Biosynthesis. *Angew. Chem., Int. Ed.* **2014**, *53*, 824−828.
(41) Schubert, H. L.; Blumenthal, R. M.; Cheng, X. Many Paths to Methyltransfer: A Chronicle of Convergence. *Trends Biochem. Sci.* **2003**, *28*, 329−335.
(42) Sun, Q.; Huang, M.; Wei, Y. Diversity of the Reaction Mechanisms of SAM-Dependent Enzymes. *Acta Pharm. Sin. B* **2021**, *11*, 632−650.
(43) Klimasauskas, S.; Timinskas, A.; Saulius, M.; Butkienè, D.; Butkus, V.; Janulaitis, A. Sequence Motifs Characteristic of DNA-[Cytosine-N4]Methyltransferases: Similarity to Adenine and Cytosine-C5 DNA-Methylases. *Nucleic Acids Res.* **1989**, *17*, 9823−9832.
(44) Kossykh, V. G.; Schlagman, S. L.; Hattman, S. Function of Pro-185 in the ProCys of Conserved Motif IV in the *Eco*RII [Cytosine-C5]-DNA Methyltransferase. *FEBS Lett.* **1995**, *370*, 75−77.
(45) Martin, J. L.; McMillan, F. M. SAM (Dependent) I AM: The S-Adenosylmethionine-Dependent Methyltransferase Fold. *Curr. Opin. Struct. Biol.* **2002**, *12*, 783−793.
(46) Pace, N. J.; Weerapana, E. Zinc-Binding Cysteines: Diverse Functions and Structural Motifs. *Biomolecules* **2014**, *4*, 419−434.
(47) Kochańczyk, T.; Drozd, A.; Krężel, A. Relationship between the Architecture of Zinc Coordination and Zinc Binding Affinity in Proteins − Insights into Zinc Regulation. *Metallomics* **2015**, *7*, 244−257.
(48) Xia, P.; Lian, S.; Wu, Y.; Yan, L.; Quan, G.; Zhu, G. Zinc Is an Important Inter-Kingdom Signal between the Host and Microbe. *Vet. Res.* **2021**, *52*, No. 39.
(49) Wątły, J.; Potocki, S.; Rowińska-Żyrek, M. Zinc Homeostasis at the Bacteria/Host Interface-From Coordination Chemistry to Nutritional Immunity. *Chem. - Eur. J.* **2016**, *22*, 15992−16010.
(50) Ye, R.; Tan, C.; Chen, B.; Li, R.; Mao, Z. Zinc-Containing Metalloenzymes: Inhibition by Metal-Based Anticancer Agents. *Front. Chem.* **2020**, *8*, No. 402.
(51) Tejwani, G. A.; Pedrosa, F. O.; Pontremoli, S.; Horecker, B. L. Dual Role of Zn2+ as Inhibitor and Activator of Fructose 1,6-

https://doi.org/10.1021/acsomega.2c04555
ACS Omega 2022, 7, 35901−35910

Bisphosphatase of Rat Liver. *Proc. Natl. Acad. Sci. U.S.A.* **1976**, *73*, 2692−2695.
(52) Velázquez-Delgado, E. M.; Hardy, J. A. Zinc-Mediated Allosteric Inhibition of Caspase-6. *J. Biol. Chem.* **2012**, *287*, 36000−36011.
(53) Huber, K. L.; Hardy, J. A. Mechanism of Zinc-Mediated Inhibition of Caspase-9. *Protein Sci.* **2012**, *21*, 1056−1065.
(54) Mayaux, J. F.; Blanquet, S. Binding of Zinc to *Escherichia coli* Phenylalanyl Transfer Ribonucleic Acid Synthetase. Comparison with Other Aminoacyl Transfer Ribonucleic Acid Synthetases. *Biochemistry* **1981**, *20*, 4647−4654.
(55) Matthews, R. G.; Goulding, C. W. Enzyme-Catalyzed Methyl Transfers to Thiols: The Role of Zinc. *Curr. Opin. Chem. Biol.* **1997**, *1*, 332−339.
(56) Evans, J. C.; Huddler, D. P.; Jiracek, J.; Castro, C.; Millian, N. S.; Garrow, T. A.; Ludwig, M. L. Betaine-Homocysteine Methyltransferase. *Structure* **2002**, *10*, 1159−1171.
(57) Gu, H. F.; Zhang, X. Zinc Deficiency and Epigenetics. In *Handbook of Famine, Starvation, and Nutrient Deprivation*; Springer International Publishing: Cham, 2017; pp 1−18.
(58) Hood, M. I.; Skaar, E. P. Nutritional Immunity: Transition Metals at the Pathogen-Host Interface. *Nat. Rev. Microbiol.* **2012**, *10*, 525−537.
(59) Marshansky, V.; Futai, M. The V-Type H+-ATPase in Vesicular Trafficking: Targeting, Regulation and Function. *Curr. Opin. Cell Biol.* **2008**, *20*, 415−426.
(60) Kükürt, A.; Gelen, V.; Başer, Ö. F.; Deveci, H. A.; Karapehlivan, M.Thiols: Role in Oxidative Stress-Related Disorders. In *Accenting Lipid Peroxidation*; IntechOpen, 2021.
(61) Hübner, C.; Haase, H. Interactions of Zinc- and Redox-Signaling Pathways. *Redox Biol.* **2021**, *41*, No. 101916.

https://doi.org/10.1021/acsomega.2c04555
ACS Omega 2022, 7, 35901−35910